NACA

RESEARCH MEMORANDUM

EXPERIMENTAL INVESTIGATION OF THE ZERO-LIFT DRAG OF A FIN-STABILIZED BODY OF FINENESS RATIO 10 AT MACH NUMBERS BETWEEN 0.6 AND 10

By Carlton S. James and Robert J. Carros

Ames Aeronautical Laboratory
Moffett Field, Calif.

NATIONAL ADVISORY COMMITTEE
FOR AERONAUTICS

WASHINGTON

June 11, 1953

NATIONAL ADIVISORY COMMITTEE FOR AERONAUTICS

RESEARCH MEMORANDUM

EXPERIMENTAL INVESTIGATION OF THE ZERO-LIFT DRAG OF A FIN-STABILIZED BODY OF FINENESS RATIO 10 AT MACH NUMBERS BETWEEN 0.6 AND 10

By Carlton S. James and Robert J. Carros

SUMMARY

Free-flight measurements were made of the zero-lift drag of a cruciform-finned body at Mach numbers between 0.6 and 10. Reynolds numbers varied between 0.9 million and 16 million. It was observed that the drag coefficient after increasing sharply through Mach number 1 drops rapidly in the low supersonic region to values well below the subcritical value. The drag coefficients at Mach numbers above 5 were less than half the M = 0.6 value, and the variation of drag coefficient with Mach number was considerably less at Mach numbers above 5 than at Mach numbers below 5.

The zero-lift drag of this model was predicted over the range of Mach numbers from 1.5 to 10 and compared with the experimental results. At Mach number 5 a maximum disagreement between theory and experiment of 18 percent occurred. Above and below this Mach number the agreement improved so that over most of the Mach number range it was within 8 percent. Accuracy of the prediction was affected principally by uncertainties in the base drag estimate at low Mach numbers and in the location of boundary-layer transition at all Mach numbers.

The effect of Reynolds number on the drag was measured at two Mach numbers, 4.7 and 7.2, and was found to be small. The ranges of Reynolds numbers covered were between 4 million and 9 million at M = 4.7 and between 7 million and 16 million at M = 7.2.

An indication was obtained from preliminary data that the effect on total drag of varying the fin leading-edge profile is small if extreme bluntness is avoided.

INTRODUCTION

In the field of missile aerodynamics there is an increasing need for experimental data at high supersonic Mach numbers for the purpose of testing the validity of existing theory at these speeds as well as for direct use in design calculations. At Mach numbers greater than 5 very little aerodynamic data have as yet been published with which theoretical predictions can be compared.

One of the fundamental parameters is the drag, which often is important in considerations of range, velocity, and missile size. It was the twofold purpose of the investigation described in this report to provide total drag data for a finned missile configuration over as wide a range of Mach numbers as possible, and to determine the degree of accuracy with which existing theoretical methods can be expected to predict the drag of this and similar configurations throughout the supersonic speed range of the test.

The importance of Reynolds number effects was examined with regard to both the applicability of the test results to other conditions and to the application of the theory in predicting drag.

During the developmental phase of the testing, some data were obtained which provide an indication of the effect on total drag of blunting the fin leading edge.

SYMBOLS

A_B base area of body, sq ft

C_D total drag coefficient, $\frac{\text{total drag force}}{A_B q}$

$C_{D_{\alpha=0}}$ total zero-lift drag coefficient

ΔC_D integrated average drag increment due to angle of attack

C_{D_b} base drag coefficient, $\frac{\text{base drag force}}{A_B q}$

C_{D_f} friction drag coefficient, $\frac{\text{friction drag force}}{A_B q}$

$C_{D_{f_{body}}}$ body-alone friction drag coefficient

C_N normal force coefficient, $\frac{\text{normal force}}{A_B q}$

M free-stream Mach number

p_b base pressure, lb/sq ft

q free-stream dynamic pressure, lb/sq ft

R Reynolds number based on free-stream properties and model length

R_T transition Reynolds number based on free-stream properties and length of run of the laminar boundary layer

t time, sec

α angle of attack, radians

$\bar{\alpha}$ mean angle of attack, $\frac{\int_{1,4} \alpha dt}{t_{1,4}}$, radians

Subscripts

1,2; 1,3; 2,3; etc. intervals of time or distance between stations 1 and 2, 1 and 3, 2 and 3, etc.

TEST TECHNIQUE AND CONDITIONS

Technique

The investigation was conducted in the Ames supersonic free-flight wind tunnel. In this facility the model is launched from a gun mounted in the wind-tunnel diffuser and flies upstream through the test section. Mach numbers below approximately 4 are obtained by firing the model through still air. Higher Mach numbers are obtained by firing through the supersonic air stream of the wind tunnel. A detailed discussion of the test technique will be found in reference 1.

Models

The model tested is shown in figure 1(a). The body has an ogive nose tangent to a circular-cylindrical afterbody. The fineness ratio of

the nose is 4 and the over-all fineness ratio is 10. The cruciform fins are trapezoidal in plan form. The basic fins have asymmetric-wedge leading-edge profiles and blunt, unswept trailing edges which are coincident with the body base. The aspect ratio of the exposed fins joined together is 0.426. The thickness ratio in terms of the local chord is constant and equal to 0.04. During the development stage of the program, data were also obtained on a few models whose fins had symmetrical-wedge- and blunt leading-edge profiles. These modifications are shown in figures 1(b) and 1(c), respectively.

A hole was drilled in the base of each model to move the center of gravity forward of the center of pressure to provide static longitudinal stability. Most of the models were constructed of 75 S-T aluminum, although a few were made of a magnesium alloy (Dowmetal O-1). The surfaces were polished with jeweler's rouge to a fair shine, care being taken not to alter the profile or round the edges of the fins. Roughness of the surface was measured on a representative group of models as a check on uniformity. Graphs of the local surface irregularities were obtained using a stylus-type profile following instrument. Typical graphs, at two magnifications, are shown in figure 2. It was concluded that the degree of roughness on these models was sufficiently uniform that any possible effects of roughness on friction drag would be consistently duplicated from one round to another.

The models were launched from .50 caliber smooth-bore guns using plastic sabots as pistons to push the models and to hold them in the proper attitude during firing. The sabots separate from the models a few feet from the gun due to aerodynamic forces. Figure 3 shows photographs of a model, sabot components, and assemblies ready for launching.

Range of Test Conditions

The test Mach number was varied between 0.6 and 10. The corresponding Reynolds number range was from 0.9 million to 16 million. The variation of Reynolds number with Mach number is shown in figure 4. It is seen that under air-off test conditions,[1] Reynolds number is proportional to Mach number. Under air-on test conditions, Reynolds number can be varied (by changing reservoir pressure) within the limits shown. Over most of the air-on Mach number range the Reynolds number was held constant at 7 million as shown in figure 4. Checks were made at Mach numbers of 4.7 and 7.2 to determine the dependence of drag on Reynolds number.

[1]Tests made in still air are referred to as "air-off," while those made with the supersonic air stream flowing through the tunnel are referred to as "air-on."

REDUCTION AND PRECISION OF DATA

Method of Obtaining Data

As a model flies through the test section approximately parallel to an Invar distance scale, spark shadowgraphs are taken at four positions along the scale. The elapsed time between spark discharges is recorded by a chronograph. From this time-distance history of the model flight, the deceleration due to drag is obtained. This, when combined with the known mass of the model, is sufficient to calculate the drag force using Newton's second law of motion. The method is fully developed in reference 1 and will, therefore, not be repeated here. A series of typical spark shadowgraphs obtained throughout the supersonic Mach number range of this investigation is presented in figure 5.[2]

Correction for Effect of Angle of Attack

Despite the desire to test the models at zero lift, small pitching oscillations of the models in flight, caused by launching disturbances, are always present. These pitching oscillations introduce small increments of drag due to angle of attack. The drag due to angle of attack was therefore estimated and subtracted from the measured total drag to obtain the zero-lift drag in accordance with the relation

$$C_{D_{\alpha=0}} = C_D - \Delta C_D \qquad (1)$$

where ΔC_D is the integrated average drag increment due to pitching. Since ΔC_D is, in turn, a function of angle of attack, the mean angle of attack $\bar{\alpha}$ was obtained by integrating the time variation of angle of attack of each round. The ΔC_D was then estimated theoretically using the relation[3]

[2]The small black rectangles appearing in the air-off shadowgraph of figure 5(c) are grains of unburned gun powder lying on the lower window of the wind tunnel, which resulted from the firing of a preceding round.

[3]A more rigorous equation is: $\Delta C_D = (\int_{1,4} C_N \alpha dt)/t_{1,4}$. The results of this equation were compared with those of equation (2) for a discarded round having nearly maximum α variation in time $t_{1,4}$ and a computed $\bar{\alpha}$ of 8.3° and were found to differ by only 4 percent of ΔC_D. Equation (2) was therefore used for all data rounds because of its simplicity.

$$\Delta C_D = C_N \bar{\alpha} \qquad (2)$$

in which the normal force coefficient C_N was calculated by one of three methods, depending on Mach number. At Mach numbers below 4, C_N was obtained using the method of Spreiter (ref. 2). At Mach numbers between 4 and 7.5, C_N was calculated using the method of Nielsen and Kaattari (ref. 3) to obtain the normal force due to the fins and fin-body mutual interference, and using the hypersonic theory of Grimminger, Williams, and Young (ref. 4) to obtain the normal force on the body. At M = 10, lift interference was neglected and reference 4 was used to calculate C_N of the combination. The dependence of drag coefficient on angle of attack was calculated using equation (2) and C_N obtained by these methods. The results are compared in figure 6 with the experimental total drag data at three Mach numbers.[4]

Precision

Possible experimental errors fall into three categories: (1) errors incurred in the angle-of-attack corrections; (2) random errors of measurement; and (3) systematic errors. These errors are discussed in the following paragraphs.

Angle-of-attack correction.- Errors due to angle-of-attack corrections were kept small by discarding most of the rounds for which $\bar{\alpha}$ exceeded 3°. A few such rounds were retained for Mach numbers at which the data were meager. The values of $\bar{\alpha}$ and of $\Delta C_D/C_{D_{\alpha=0}}$ for all rounds used are listed in table I. With six exceptions (all air-on), the ratios of ΔC_D to corrected total drag are less than 0.1. It is estimated that the drag increments have been obtained within an accuracy of ±25 percent. The resulting zero-lift drag for most rounds should therefore be in error by no more than 2-1/2 percent due to angle of attack. At M = 10, where the maximum correction of 46 percent occurs (85 percent of $C_{D_{\alpha=0}}$), the possible error could be as high as 21 percent of $C_{D_{\alpha=0}}$. It is expected that the actual errors lie well within these limits.

Random errors.- The four values of C_D calculated from the redundant data of each round (see ref. 1 for details) differ somewhat due, primarily, to inaccuracies of measurement of time and distance. The arithmetic

[4]In order to eliminate small Mach number effects due to scatter of data about a chosen average Mach number, the data were adjusted by an amount $\partial C_D/\partial M(M_{average}-M)$. The values of $(M_{average}-M)$ were, in all cases, less than 0.08.

mean is therefore taken as the correct value for the round. The scatter about this mean value is a measure of the relative uncertainty due to random causes within a round. This averages about ±3 percent for all rounds. Table I gives the maximum scatter for each round.

The net magnitude of error in a group of rounds due to random causes, such as errors in measurement, variation of model dimensions, etc., is indicated by the scatter of data points from a faired curve of $C_{D_{\alpha=o}}$ vs M. At M = 2 the average scatter is less than ±2 percent of $C_{D_{\alpha=o}}$ while at M = 10 it is ±10 percent.

Systematic errors.- The sum of small systematic errors introduced in the measurement of time and distance, air temperature and pressure, and model weight was estimated to be less than 1 percent.

A potential source of systematic errors near Mach number 7 was the deformation of models due to high stresses from the acceleration of launching. At Mach numbers below 7, the stresses of launching were safely below the strength of the material. The data at Mach number 10 were obtained using a longer barreled gun, which became available near the end of the test program, so that the launching stresses were within safe limits here also. At M = 7.2, however, it was evident from the shadowgraphs and a few recovered models that the launching stresses were sufficient to deform some of the models, and it was necessary to discard the data from these rounds.

THEORETICAL CONSIDERATIONS

The zero-lift drag of the configuration was estimated by summing up the component drag forces calculated using various theories. The total drag was considered to be made up of head drag (nose wave drag), fin wave drag, friction, and base drag.

Head Drag

Values of the head drag of ogives were computed in references 5 and 6 by the method of characteristics and were correlated in these references using the hypersonic similarity rule. The values of head drag used here were taken directly from reference 6 for Mach numbers up to 8. The value of the hypersonic similarity parameter associated with this model at a Mach number of 10 is beyond the range covered in reference 6. Therefore, the conical-shock-expansion theory (refs. 7 and 8) was used to estimate the wave drag at this Mach number.

Fin Wave Drag

The fin wave drag was estimated by integrating pressure distributions obtained by the method of Jones (ref. 9). The contribution of the opposite fin was not considered because, due to the separation of wing panels by the body, carry-over was possible only at Mach numbers less than 1.5. The effect of interference between adjacent wing panels was believed to be small, particularly because of the half-wedge profile of the leading edge, and was ignored.

Friction Drag

The skin-friction drag was calculated using the theory of Chapman and Rubesin (ref. 10) for laminar flow and that of Van Driest (ref. 11) for turbulent flow.

Body friction.- These theories were applied on the model body by assuming the average friction coefficient on the body to be the same as on a flat plate at the same free-stream Reynolds number. The effect of the initial thickness of the turbulent boundary layer at transition was accounted for by calculating an origin for a fully turbulent boundary layer which would have the same thickness as the laminar boundary layer at transition. The Reynolds number limits of the turbulent region were then based on the length of run from the hypothetical turbulent origin. The skin temperature used in the calculations was the prefiring temperature of the models (room temperature). This choice was based on calculations which indicated that, during the extremely short flight in the wind tunnel (1/100 to 1/20 second), virtually no temperature rise takes place at the model surface.

By use of this approach, the dependence of body friction on transition location was calculated at three representative Mach numbers with Reynolds numbers corresponding to those of the test. These results are plotted in figure 7. It is evident from the figure that the ability to predict the location of transition is important to the estimation of C_{D_f}. At low Mach numbers, an approximately fourfold increase in C_{D_f} occurs as the boundary layer changes from all laminar to all turbulent. At $M = 8$, the increase is threefold. In order to obtain the best possible estimates of skin friction, transition data obtained by studying the test shadowgraph pictures were used. The estimated skin friction is therefore not a purely theoretical result. The transition data were obtained at Mach numbers between 1.5 and 3 but were applied at all Mach numbers above 1.5. The locus of the applied experimental value of R_T/R as a function of Mach number is shown in the figure.

Fin friction.- The skin friction of the fins was calculated assuming the same value of R_T as was obtained for the body. The effect of immersion of the fin root in the body boundary layer was ignored; however, transverse contamination of the laminar fin boundary layer by the turbulent body boundary layer was assumed to occur. The contamination was assumed to originate at the fin-root leading edge and, at Mach numbers below 6, to propagate at an angle of 9-1/2° from the stream direction.[5] At Mach numbers greater than 6, the Mach angle is less than 9-1/2°. Since the effect of this condition on the rate of transverse propagation is not known, the rate was assumed to remain unchanged. At Mach numbers above 7, in any event, the area affected by contamination was largely blanketed by turbulent boundary layer due to transition, thereby minimizing the possible error due to this assumption. With the transition boundary thus estimated, the theories of references 10 and 11 were applied in the same manner as on the body. The calculated values of skin friction so obtained were about one third to one half as large as the body friction.

Total skin friction.- The total estimated skin friction as a function of Mach number is shown in figure 8 as the solid curve. The discontinuities which appear at $M = 4$ and $M = 7.2$ are due to changes in the test conditions. As indicated in figure 4, the Reynolds number changes discontinuously at these two Mach numbers. At $M = 4$, there is also a change in stagnation temperature from 2200° Rankine air-off to 1200° Rankine air-on.

Evaluation of method.- In order to evaluate the errors introduced by directly applying these two-dimensional theories to this three-dimensional body, the procedure described was compared to a second more rigorous one by applying both to the special case in which transition was assumed to occur at the nose-body juncture ($R_T/R = 0.4$ in fig. 7) at all Mach numbers. In the second method, the Hantzsche and Wendt theory for laminar flow on cones (ref. 13) was applied to the ogive. Local Reynolds number was used instead of free-stream Reynolds number. To obtain the local Reynolds number required, the average values of density and velocity on the ogive were used. Flow over the cylinder and the fins was treated as two-dimensional. As before, allowance was made for the initial thickness of the turbulent boundary layer at transition, and the line of transition on the fins was defined in the same manner.

[5]This is the angle determined experimentally for subsonic flow by Charters in reference 12. A few observations, using the China-clay technique, of the phenomenon at Mach numbers between 1.5 and 3 were made during some tests conducted in the Ames 1- by 3-foot supersonic wind tunnels No. 1 and No. 2 in which transition was induced by several means. These included a wire trip, wing-body intersection, and a speck on the flat surface of a wing. The observed angles of propagation agreed approximately with that found for subsonic flow.

Curves of the friction drag coefficient obtained by the two methods are compared in figure 8. The results agree within 3 percent below $M = 7.2$ and within 8 percent above $M = 7.2$, indicating that little advantage is to be gained by use of the second method which although more rigorous is also more tedious. The proximity of these two curves to the solid curve is fortuitous and only indicates that the assumption of transition at the shoulder gives a close estimate of C_{D_f} for this particular investigation. This can be verified by reference to figure 7.

Base Drag

Because of the lack of an adequate theoretical approach to the estimation of base drag of bodies with fins, the present estimate was based on experimental data (refs. 14 through 19) together with the limiting curve given by $p_b = 0$. Data for both finned and finless bodies were considered. It has been demonstrated (ref. 19) that the presence of fins at or near the base of a body can have a strong influence on base pressure, at least at low supersonic Mach numbers. Such parameters as plan form, thickness ratio, and number of fins have also been shown to significantly affect base drag. In addition to these parameters, one would expect fin trailing-edge-profile shape to be important, particularly when data involving sharp and blunt trailing edges are compared. Available data in the low Mach number range of interest (i.e., $1.5<M<2$, approximately) are too meager to permit any attempt at correlation of these effects. One other effect - the influence which the hollow base may have on the base drag - is not clearly understood. The small amount of existing experimental evidence in this connection (e.g., ref. 18) would seem to indicate that, for slightly supersonic Mach numbers at least, a small reduction in base drag is to be expected when the solid base is replaced by a hollow chamber. However, no explicit consideration of this effect has been made in the present estimate.

The base drag data on which the present estimate is based are shown in figure 9 plotted against Mach number. These data cover a wide range of values in the low supersonic Mach number range. On the other hand, as Mach number increases, all the data - for finned and finless bodies alike - appear to converge toward a single curve or narrow band. Accordingly, a probable curve has been faired which averages the finned body data at the low Mach number end, but favoring somewhat the configuration most closely approximating the present one (ref. 18). Above Mach number 6.5 it was necessary to extrapolate the curve. The extrapolation was based on the limiting curve and the assumed condition that at the highest Mach numbers $C_{D_b}/(C_{D_b})_{max} \approx \text{const.} = 0.9$. The base pressure on the fins was assumed equal to that on the body because, with a span-diameter ratio of 2, it would be expected that the inflow from the tip and from the body

base region would so modify the two-dimensional fin base pressure as to cause it to approximate the body base pressure.

Summation of Component Drags

Figure 10 shows the summation of the component drags, obtained by the foregoing methods, and the resulting estimate of total zero-lift drag. It is seen that the largest contribution to the drag at low Mach numbers is the base drag, which controls the shape of the total drag curve in this region. At the higher Mach numbers, while the slope of the total drag curve is still influenced primarily by the base drag, since the rate of change with Mach number of the other components is small, skin friction and head drag become the largest components percentagewise.

RESULTS AND DISCUSSION

Experimental Total Drag

The experimental curve of zero-lift drag coefficient, $C_{D_{\alpha=0}}$, versus Mach number is plotted in figure 11. The essential features of the curve are that the drag coefficient, from subcritical Mach numbers, increases sharply through $M = 1$ to a maximum and then drops rather rapidly in the low supersonic region to values well below the subcritical value. Above Mach number 5 the curve flattens out and the slope appears to slowly approach zero. The slope of the curve through $M = 1$ and the peak value of $C_{D_{\alpha=0}}$ are not well defined because of insufficient data in this region and, further, because no corrections have been applied for effects of tunnel-wall interference at subsonic and transonic Mach numbers.[6] The large "bucket" appearing in the curve at $M = 1.5$ is believed due to variation of the base drag. This phenomenon will be discussed later in some detail.

The data near $M = 7.2$ appear high when compared with adjacent points. As explained earlier, this is the Mach number at which structural failure occurred on several models. Shadowgraphs of the rounds which were retained showed no evidence of failure; however, it is possible that small deformations - yet large enough to have appreciably affected the drag - could not have been detected from the shadowgraphs. For this

[6] It is believed that such corrections would have been small because the ratio of model cross-sectional area to tunnel cross-sectional area was of the order 10^{-4} and the minimum distance to any wall was 10 times the maximum fin span. Supersonic rounds for which the reflected bow wave intersected the model were not used.

reason, and because of the large drag-due-to-lift corrections required at $M = 10$, the uncertainty in the experimental curve above $M = 7$ is greater than at the lower Mach numbers.

Comparison of Theory with Experiment

The theoretical variation of drag with Mach number is compared with the experimental data in figure 12. The comparison shows that the experimental drag is reasonably well predicted by theory. The largest percentage discrepancy occurs in the region of Mach number 5, where the predicted $C_{D_{\alpha=0}}$ is about 18 percent above the mean value of the experimental points. Through the Mach number range 1.5 to 3, the prediction agrees with experiment within 5 percent. This good agreement is to some degree fortuitous because the uncertainty in the base drag estimate is of the same order of magnitude. At Mach number 10 the theoretical prediction overestimates the experimental value by about 5 percent. This is within the accuracy of the experiment at this Mach number.

Comparison of Experiment with NOL Results

Force measurements on a model nearly identical to the one tested here have been made in the 40- by 40-centimeter wind tunnels of the Naval Ordnance Laboratory[7] and are reported in references 20 and 21. The results of these measurements are compared with the present results in figure 13. In general, the NOL results indicate a more rapid decrease of drag coefficient with increasing Mach number than do the present results, and a maximum disagreement of 20 percent occurs at Mach number 3.5. Although the cause of the disagreement is not known, it is possible to account for differences of this magnitude on the basis of differences in stream Reynolds number and transition Reynolds number. This can be demonstrated quickly with the aid of figures 4 and 7. If, for example, the Mach number is chosen at which for both tests the Reynolds number is the same ($M = 2.4$; $R = 3.6$ million), figure 7 indicates that the difference in measurements of the total drag might be completely accounted for by a difference in transition Reynolds numbers.

Boundary-Layer Transition

Transition was observed on a number of the air-off shadowgraphs. One such shadowgraph is shown in figure 14 for which the Mach number was

[7]The only violation of geometrical similarity is that the model of the present investigation had fins tapered in thickness to give a constant thickness ratio, while the NOL model had fins of constant thickness equal to 3.13 percent of the root chord.

3.29, and the Reynolds number of the free stream was 4.9×10^6. Transition is indicated by the arrows. For these rounds, transition Reynolds number R_T was determined and plotted against free-stream Reynolds number R. The results are shown in figure 15. The diameter of the circles indicates the estimated accuracy of the measurements which is rather poor, due to uncertainty in picking the transition point and because the position of this point was found to vary with time, angle of attack, and meridian position. Within the accuracy of the data, transition Reynolds number is shown for this limited range ($2.9 \times 10^6 < R < 5 \times 10^6$) to be independent of the free-stream Reynolds number and to have a value of approximately 1.6 million. This value is low in comparison with usual wind tunnel and free-flight experience. The reason for this early transition is not clear, particularly since the low temperature of the skin relative to stagnation temperature would lead to the expectation of transition at a relatively high Reynolds number. Stream turbulence is not a factor since the data of figure 15 were obtained for models flying through still air. It is possible that surface roughness of the models was sufficient to lower the transition Reynolds number.

Location of transition by inspection of the air-on shadowgraphs is extremely uncertain, largely because the body boundary layer is obscured in the picture by turbulence in the boundary layer on the wind-tunnel windows. As well as can be determined, transition occurs in some cases at the Reynolds number determined from the air-off shadowgraphs, while in others there is evidence that some laminar flow exists at local Reynolds numbers as high as 8 or 10 million.[8] For lack of a more definitely determined value in this test range, the air-off value of transition Reynolds number was assumed in the theoretical calculations to apply over the air-on range as well. If, instead, at Mach number 10 transition should be found to occur at a Reynolds number of 10 million, the theoretical drag coefficient would be reduced by about 14 percent. Similarly, in the region of Mach number 5, it would be possible to account for the entire discrepancy between the predicted and experimental values of drag coefficient if transition were assumed to occur at a Reynolds number of 7 million instead of 1.6 million. It is evident from these considerations that a better understanding of the manner in which boundary-layer transition is affected by other conditions would result in a more accurate prediction of friction drag and, hence, total drag. Further research in this direction is needed.

The bucket in the total drag curve at $M = 1.5$ (fig. 11) is a rather surprising phenomenon for which no definite explanation has been found. It is believed to be a base drag effect resulting from the combined

[8]See, for example, figures 5(e) and 5(f). Note the turbulent "bursts" along the body, each of which is revealed by a weak shock wave at its leading edge. In figure 5(f) one prominent shock wave from a burst is indicated by an arrow.

effects of transition shift across the base of the model and the influence of the fin shock waves. In reference 22, Chapman showed that for similar bodies without fins the difference between laminar and turbulent base drag coefficients at a Mach number of 1.5 and Reynolds number of 2.0 million was 0.04. In the present test the change in drag coefficient at $M = 1.5$ was approximately 0.04. Furthermore, it is the Mach number range between approximately 1.5 and 2 in which the Mach lines from the fin-tip leading edges sweep across the model base. It seems at least plausible, therefore, that the vertical side of the bucket may be associated with transition shift, while the horizontal side may be associated with the influence of the fins. Only one piece of evidence has been found which does not agree well with the foregoing hypothesis: At Mach number 1.5, the Reynolds number at the body base is 2.2 million which, to be consistent, should correspond to boundary-layer transition. This value is somewhat higher than the transition Reynolds number of 1.6 million obtained at higher stream Reynolds numbers (see fig. 15).

Reynolds Number Effects

The effect of Reynolds number on the total drag was found to be small at the two Mach numbers where checks were made. Figure 16 shows the change in the total drag coefficient at Mach numbers of 4.7 and 7.2 when the Reynolds number is approximately doubled from 4.0 million and 7.2 million, respectively. The following changes in the viscous flow would be expected to occur with increasing Reynolds number:

1. Forward movement of transition, increasing the ratio of turbulent wetted area to laminar wetted area and tending to increase the drag coefficient

2. Decrease in the average turbulent shear coefficient because of the increased Reynolds number of the turbulent run, tending to decrease the drag coefficient

3. Slight decrease in the friction drag coefficient of the fins

4. Slight reduction of the base drag coefficient

Apparently, in the present case, the compensation of these effects is nearly complete. At lower Mach numbers, or where R_T/R varies over a wide range, increased sensitivity of drag coefficient to changes in free-stream Reynolds number might occur.

Fin Leading-Edge Shape

The effects on the total drag of two changes in fin leading-edge profile were determined from a number of models fired during launching development. One profile (fig. 1(b)) is symmetrically beveled at a 20° half angle measured in a plane normal to the leading edge. The other profile (fig. 1(c)) is blunt, being composed of elements of the surface of revolution formed by rotating the fin plan form about the body axis. The total drags of these configurations are compared with that of the basic configuration in figure 17. Replacing the basic leading edge with the symmetrical bevel is seen to have almost no effect on the total drag, while replacing the basic leading edge with the blunt leading edge results in a nearly constant incremental increase of about 0.02 in total drag coefficient at Mach numbers below 5. This corresponds to an increase of 4 to 10 percent in total drag coefficient, depending on Mach number. If the increase is attributed entirely to the change in fin wave drag, however, it represents an increase in fin wave drag of 100 percent. It appears from this consideration that small changes in fin leading-edge profile do not significantly affect the total drag of the configuration.

CONCLUDING REMARKS

Free-flight total drag data have been presented for a finned missile configuration at Mach numbers between 0.6 and 10, and Reynolds numbers between 0.9 million and 16 million. It was found that at Mach numbers above 5, the drag coefficients are less than half the $M = 0.6$ value and the variation of drag coefficient with Mach number is considerably less in this range than it is in the Mach number range below 5. At Mach numbers of 4.7 and 7.2 it was shown experimentally that the drag coefficient was affected only slightly by changes in Reynolds number. It was also indicated experimentally that the shape of the fin leading-edge profile need not be an important consideration in minimizing drag so long as extreme bluntness is avoided.

Comparison of the theoretically predicted drag with the experimental data in the Mach number range 1.5 to 10 indicated that the zero-lift drag of missiles generally similar to the test model can be estimated by the use of existing theory and existing base pressure data with reasonable accuracy throughout the range of comparison. In the present example a maximum error of 18 percent occurred near Mach number 5. Below $M = 4$ and above $M = 7$ the error reduced to less than 8 percent. The two principal causes of uncertainty in the estimate are the effects of fins on the base drag at low supersonic speeds and the location of boundary-layer transition throughout the speed range.

Ames Aeronautical Laboratory
National Advisory Committee for Aeronautics
Moffett Field, Calif.

REFERENCES

1. Seiff, Alvin, James, Carlton S., Canning, Thomas N., Boissevain, Alfred G.: The Ames Supersonic Free-Flight Wind Tunnel. NACA RM A52A24, 1952.

2. Spreiter, John R.: The Aerodynamic Forces on Slender Plane- and Cruciform-Wing and Body Combinations. NACA Rep. 962, 1950. (Supersedes NACA TN 1897)

3. Nielsen, Jack N., and Kaattari, George E.: Method for Estimating Lift Interference of Wing-Body Combinations at Supersonic Speeds. NACA RM A51J04, 1951.

4. Grimminger, G., Williams, E. P., and Young, G. B. W.: Lift on Inclined Bodies of revolution in Hypersonic Flow. Jour. Aero. Sci., vol.17, no. 11, Nov. 1950, pp. 675-690.

5. Ehret, Dorris M., Rossow, Vernon J., and Stevens, Victor I.: An Analysis of the Applicability of the Hypersonic Similarity Law to the Study of Flow About Bodies of Revolution at Zero Angle of Attack. NACA TN 2250, 1950.

6. Rossow, Vernon J.: Applicability of the Hypersonic Similarity Rule to Pressure Distributions which Include the Effects of Rotation for Bodies of Revolution at Zero Angle of Attack. NACA TN 2399, 1951.

7. Eggers, A. J., Jr., and Savin, Raymond C.: Approximate Methods for Calculating the Flow About Nonlifting Bodies of Revolution at High Supersonic Airspeeds. NACA TN 2579, 1951.

8. Ehret, Dorris M.: Accuracy of Approximate Methods for Predicting Pressures on Pointed Nonlifting Bodies of Revolution in Supersonic Flow. NACA TN 2764, 1952.

9. Jones, Robert T.: Thin Oblique Airfoils at Supersonic Speed. NACA Rep. 851, 1946.

10. Chapman, Dean R., and Rubesin, Morris W.: Temperature and Velocity Profiles in the Compressible Laminar Boundary Layer with Arbitrary Distribution of Surface Temperature. Jour. Aero. Sci., vol. 16, no. 9, Sept. 1949, pp. 547-565.

11. Van Driest, E. R.: Turbulent Boundary Layer in Compressible Fluids. Jour. Aero. Sci., vol. 18, no. 3, March 1951, pp. 145-160.

12. Charters, Alex C.: Transition Between Laminar and Turbulent Flow by Transverse Contamination. NACA TN 891, 1943.

13. Hantzsche, W., and Wendt, H.: The Laminar Boundary Layer on a Circular Cone at Zero Incidence in a Supersonic Stream. Ministry of Supply, Volkenrode, MOS 115, Aug. 1946.

14. Hill, Freeman K., and Alpher, Ralph A.: Base Pressures at Supersonic Velocities. Jour. Aero. Sci., vol. 16, no. 3, March 1949, pp. 153-160.

15. Douglas Aircraft Co. Missiles Tech. Memo. 24M. XAAM-N-2 Sparrow Flight Test Report, Flight No. 0028, Test Group No. 6, Missile Serial No. 0028, Launched 25 August 1949, U.S. Naval Air Missile Test Center, Point Mugu, California, Sept. 15, 1949.

16. Charters, A. C. and Turetsky, R. A.: Determination of Base Pressure from Free-Flight Data. Aberdeen Ballistic Res. Lab. Rep. 653, March 1948.

17. Hill, F. K.: Base Pressures at a Mach Number of 5.1. Johns Hopkins University A.P.L. Rep. CF-1306, July 11, 1949.

18. Peck, Robert F.: Flight Measurements of Base Pressure on Bodies of Revolution with and without Simulated Rocket Chambers. NACA RM L50I28a, 1950.

19. Spahr, J. Richard, and Dickey, Robert R.: Effect of Tail Surfaces on the Base Drag of a Body of Revolution at Mach Numbers of 1.5 and 2.0. NACA TN 2360, 1951.

20. Monahan, T. G.: Aeroballistic Research Investigation of the 0.325 Scale Model of the Surface-to-Air Missile, Zeus (XSAM-N-8), at Mach Numbers of 4.38 and 2.48. Naval Ordnance Laboratory Memorandum 10102, 12 August 1949.

21. Nestingen, I. M.: Aeroballistic Research Investigation of the 0.325 Scale Model of the Surface-to-Air Missile Zeus (XSAM-N-8) at Mach Numbers of 1.57, 1.88, 2.48, and 3.25. Naval Ordnance Laboratory Memorandum 10100, 19 August 1949.

22. Chapman, Dean R.: An Analysis of Base Pressure at Supersonic Velocities and Comparison with Experiment. NACA TN 2137, 1950.

TABLE I.- TABULATION OF EXPERIMENTAL SCATTER AND ANGLE-OF-ATTACK CORRECTIONS FOR BASIC CONFIGURATION

M	R, millions	Scatter in C_D, percent	$\bar{\alpha}$, deg	$\Delta C_D/C_{D_{\alpha=0}}$
0.598	0.86	4.4 -3.8	2.8	0.043
.901	1.28	.4 -.6	2.3	.029
1.06	1.54	2.1 -4.0	1.0	.004
1.32	1.9	1.5 -1.2	1.7	.011
1.46	2.2	3.5 -3.2	1.5	.010
1.48	2.1	.8 -1.2	1.8	.013
1.53	2.2	2.0 -1.2	1.4	.008
1.57	2.3	1.7 -.8	1.6	.011
1.58	2.3	2.3 -2.9	.6	.002
1.95	2.9	.8 -1.7	1.5	.010
2.09	3.2	.9 -1.2	2.4	.027
2.30	3.5	1.9 -2.6	2.9	.043
2.56	3.8	1.1 -1.6	1.8	.017
2.91	4.3	1.1 -1.9	.9	.005
3.29	4.9	5.9 -4.7	3.2	.068
3.99	6.6	.2 -.2	2.7	.060
4.04	6.8	1.0 -2.0	.8	.006
4.57	7.5	.4 -.3	1.8	.021
4.57	6.9	.6 -.5	1.5	.022
4.64	4.2	4.1 -1.2	3.7	.153
4.68	4.2	7.6 -7.7	1.2	.014

TABLE I.- TABULATION OF EXPERIMENTAL SCATTER AND ANGLE-OF-ATTACK CORRECTIONS FOR BASIC CONFIGURATION - Concluded

M	R, millions	Scatter in C_D, percent	$\bar{\alpha}$, deg	$\Delta C_D/C_{D_{\alpha=0}}$
4.72	4.3	4.1 -4.2	2.9	0.090
5.33	6.7	2.9 -2.4	3.8	.176
5.43	7.0	1.8 -1.3	4.1	.204
5.49	7.0	2.7 -2.6	2.8	.087
7.18	7.1	5.4 -2.3	1.6	.027
7.19	7.3	8.0 -10.0	3.3	.100
7.21	15.0	2.7 -4.1	1.0	.009
7.29	15.6	2.0 -2.6	2.9	.085
10.0	15.9	3.0 -2.6	5.9	.411
10.0	16.0	.8 -.9	8.3	.846

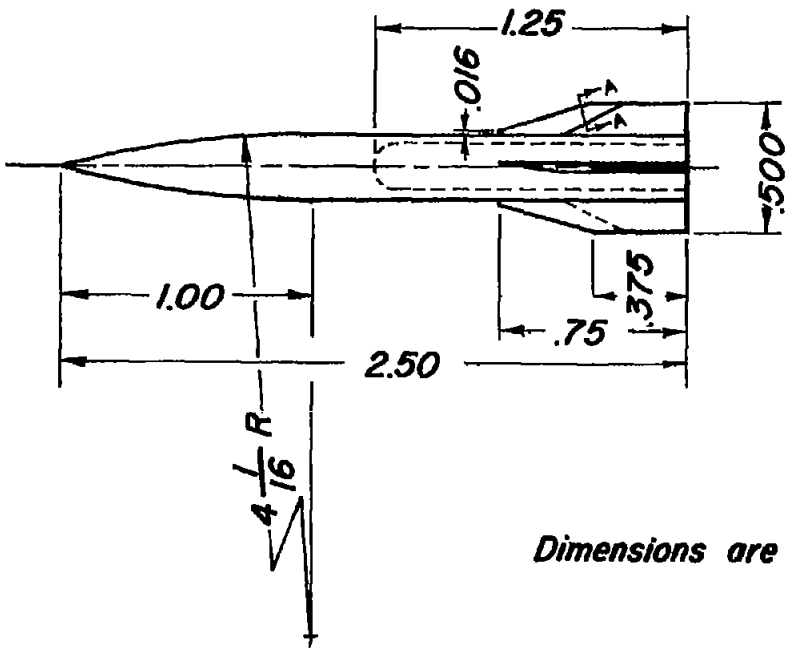

Dimensions are in inches

(a) Basic model.

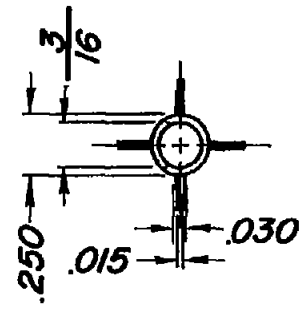

Section A-A

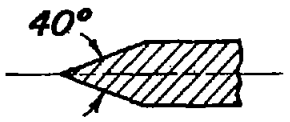

(b) Modified section A-A

(c) Modified section A-A.

Figure 1. – Sketch of test configuration.

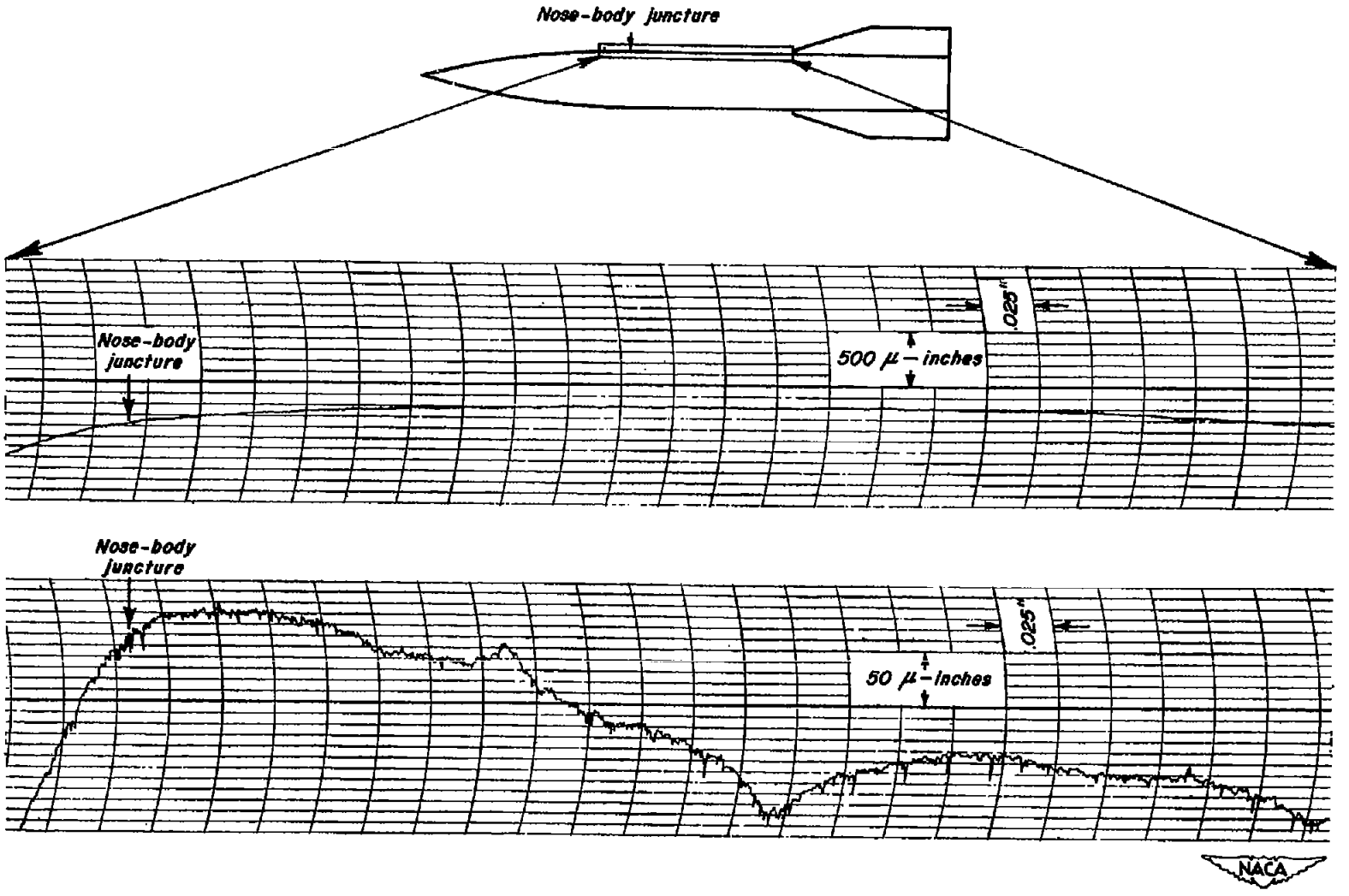

Figure 2.—Typical profiles at two magnifications of the surface roughness obtained on the cylindrical portion of two models.

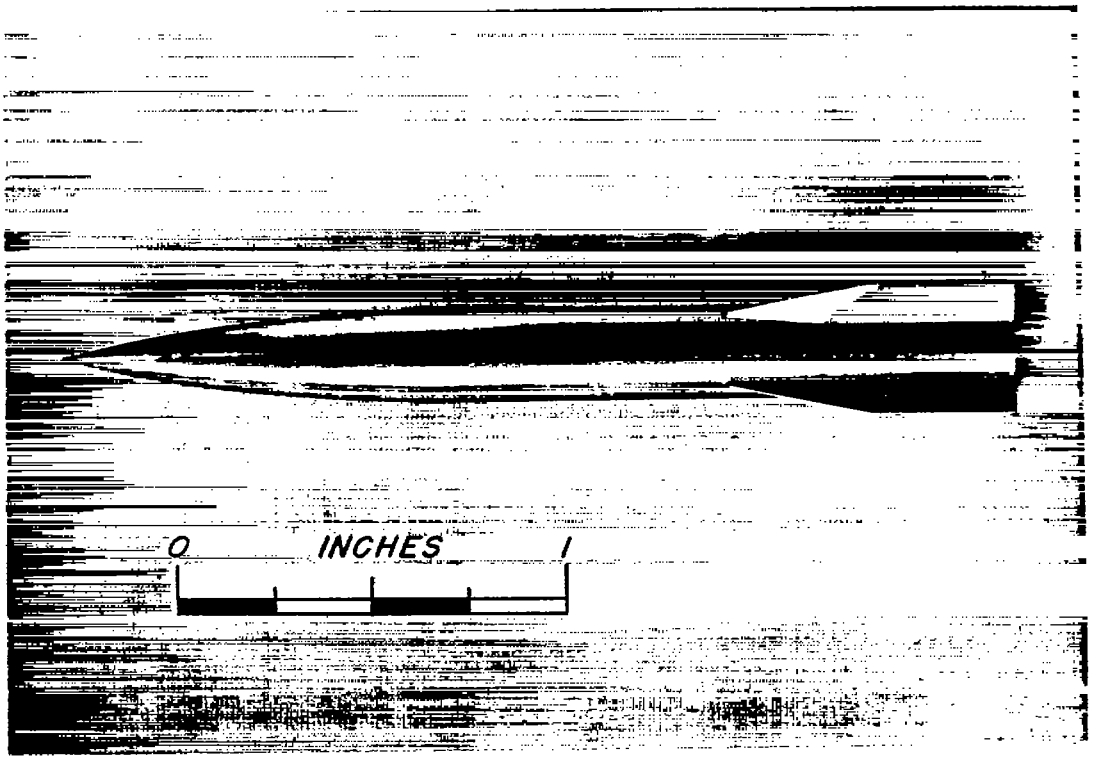

(a) Model.

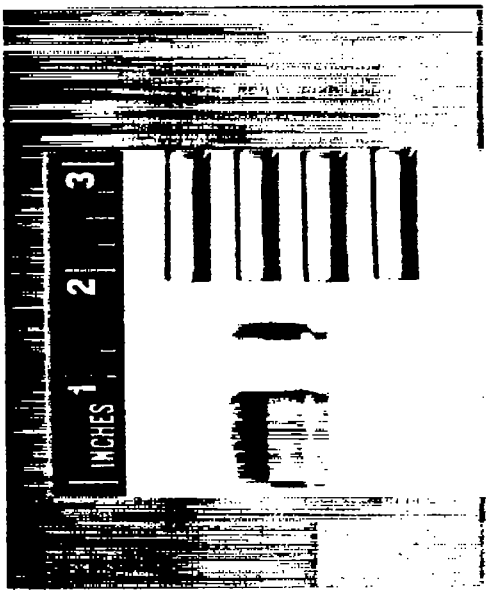

(b) Sabot.

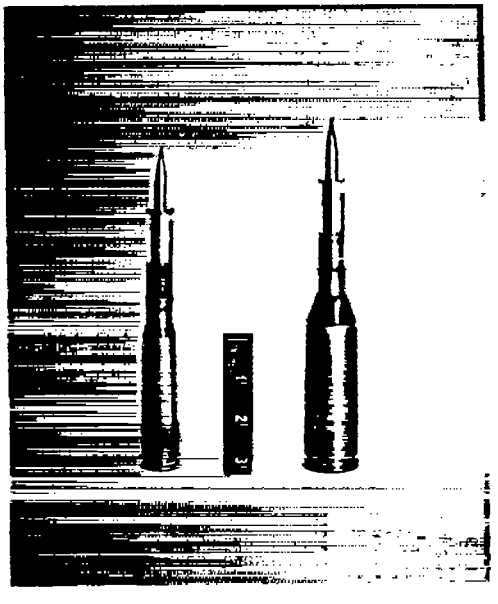

(c) Assemblies.

Figure 3.- Model, sabot, and launching assemblies.

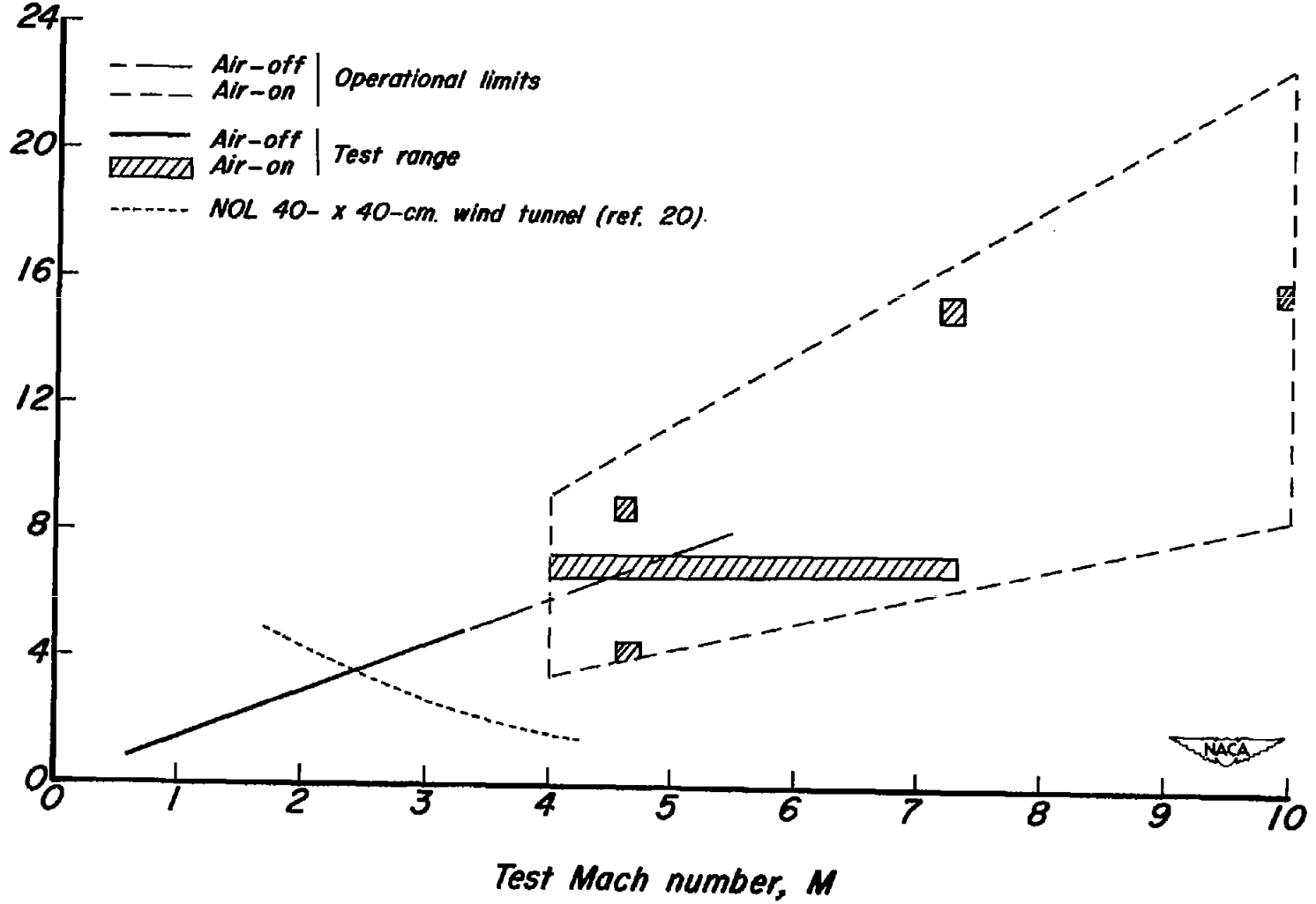

Figure 4.- Range of test Mach number and Reynolds number.

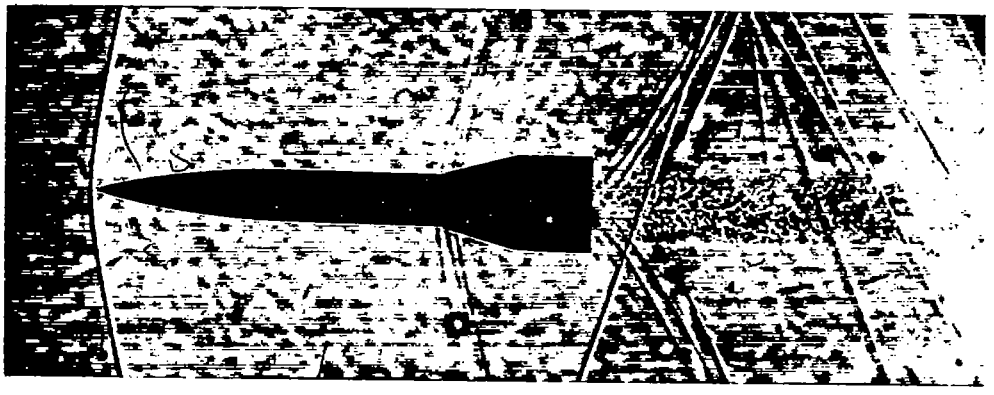

(a) M = 1.06; R = 1.5×10^6; air off

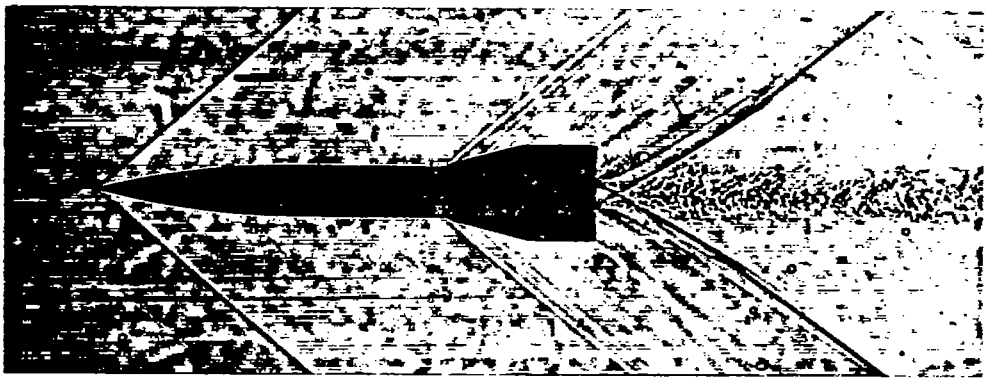

(b) M = 1.58; R = 2.3×10^6; air off

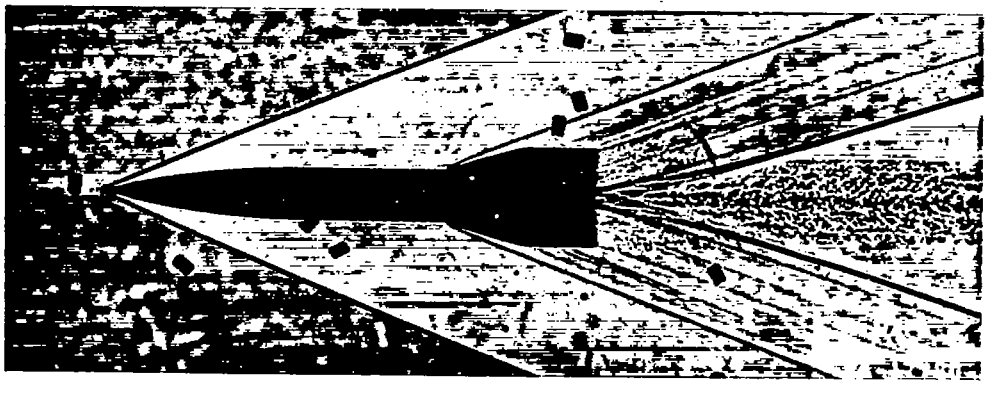

(c) M = 2.91; R = 4.3×10^6; air off

Figure 5.- Shadowgraphs of models in flight.

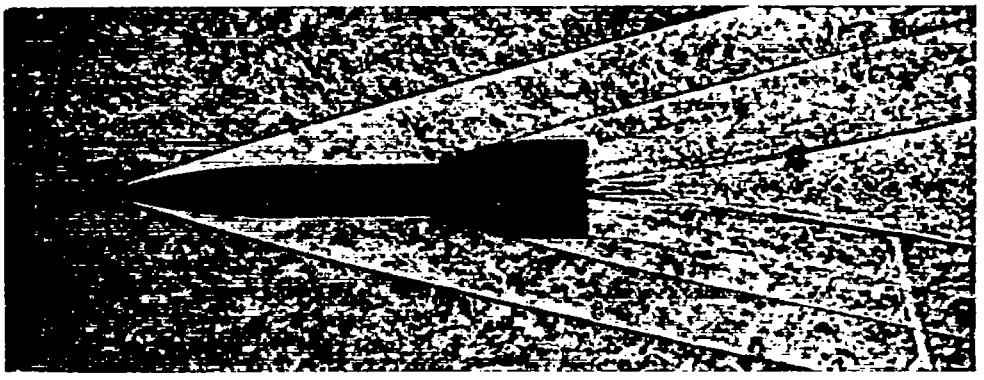

(d) M = 4.70; R = 4.1×10^6; air on

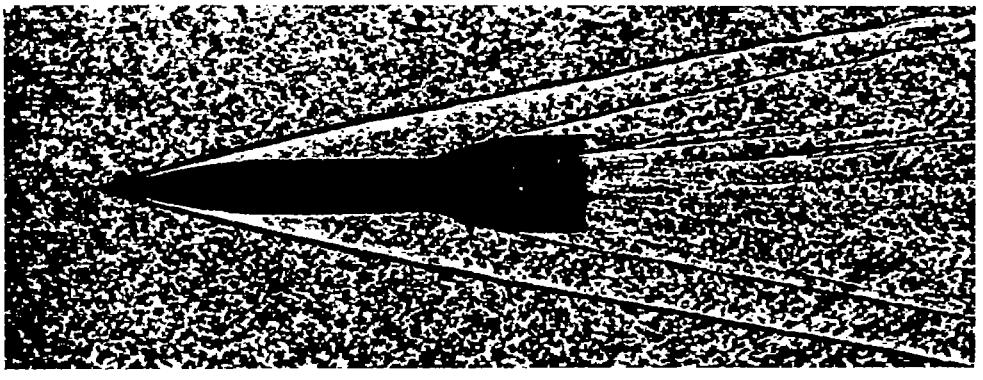

(e) M = 6.84; R = 11×10^6; air on

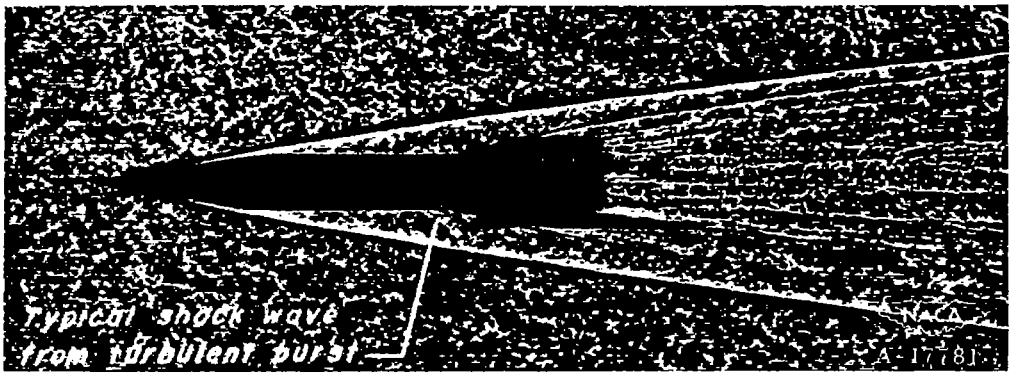

(f) M = 10.0; R = 16×10^6; air on

Figure 5.- Concluded.

[redacted]

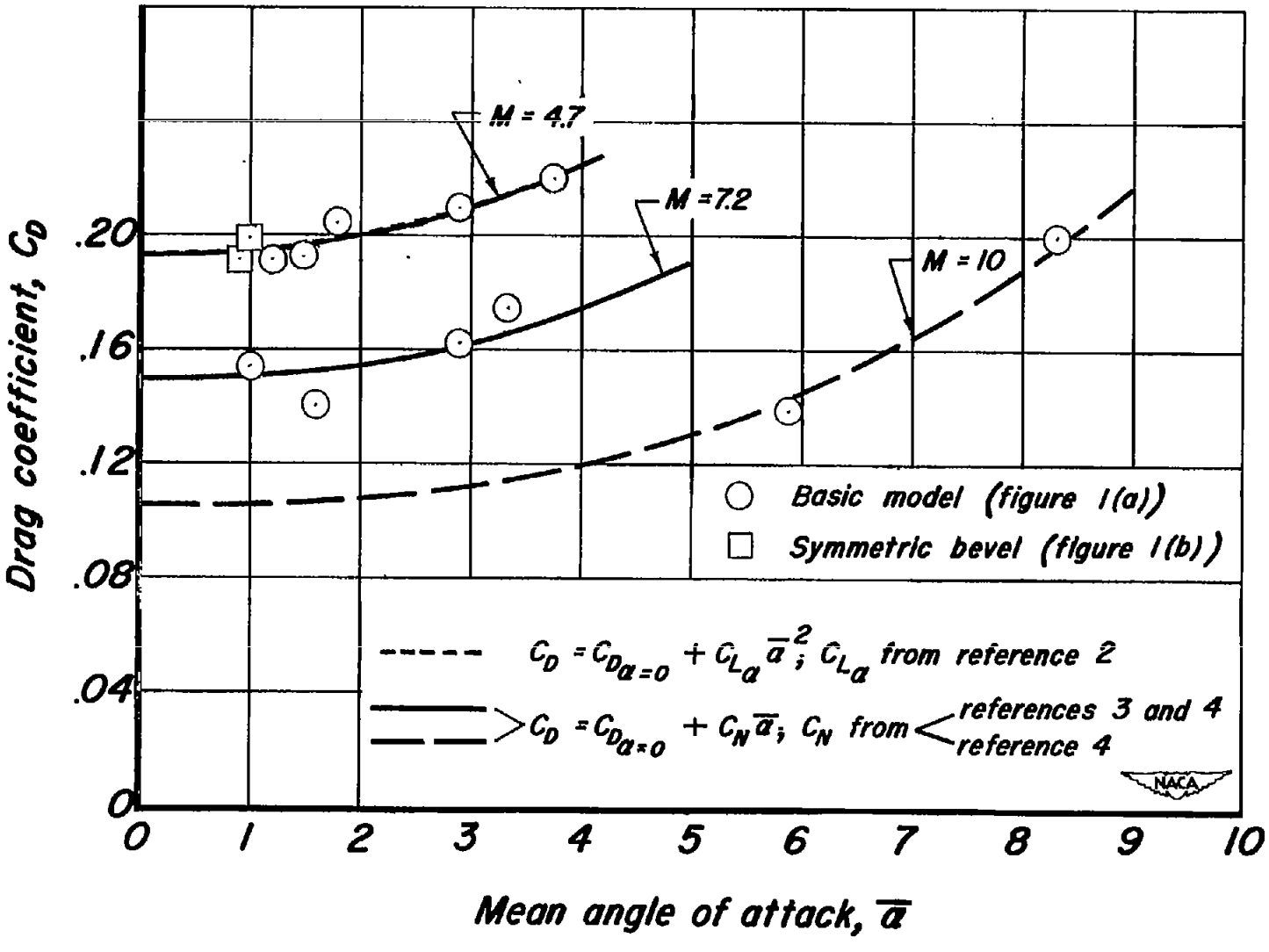

Figure 6. – Variation of total drag coefficient with angle of attack.

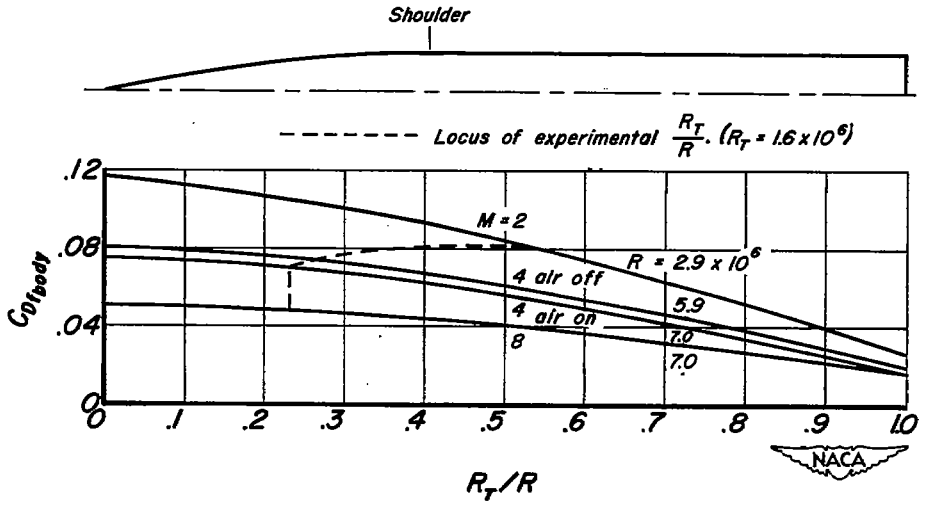

Figure 7.— Variation of theoretical body-alone friction drag coefficient with location of boundary-layer transition.

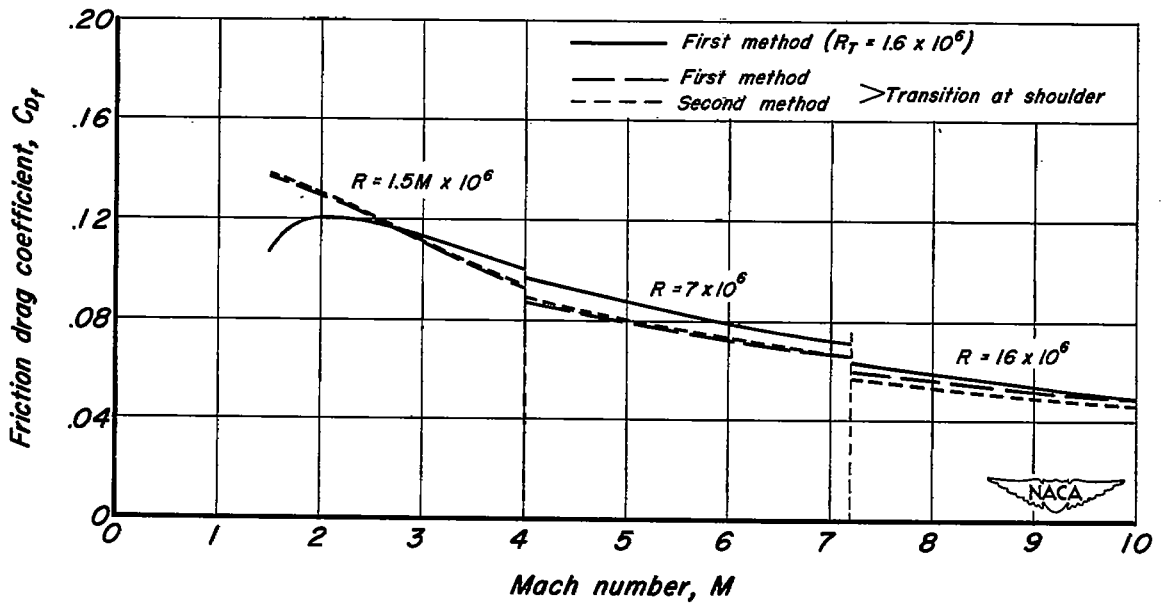

Figure 8.– Theoretical friction drag coefficient as a function of Mach number.

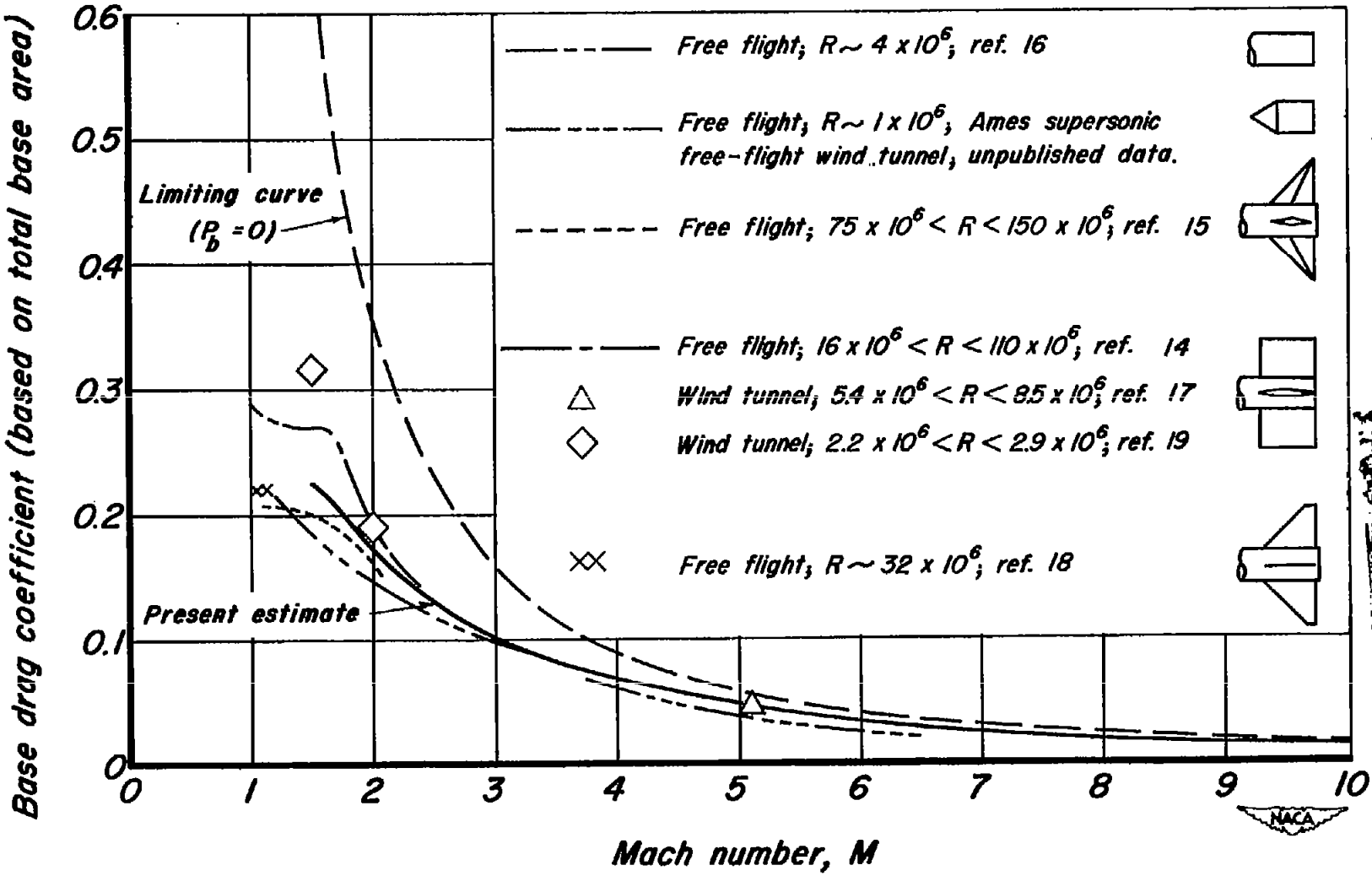

Figure 9.– Compilation of data used in estimating base drag.

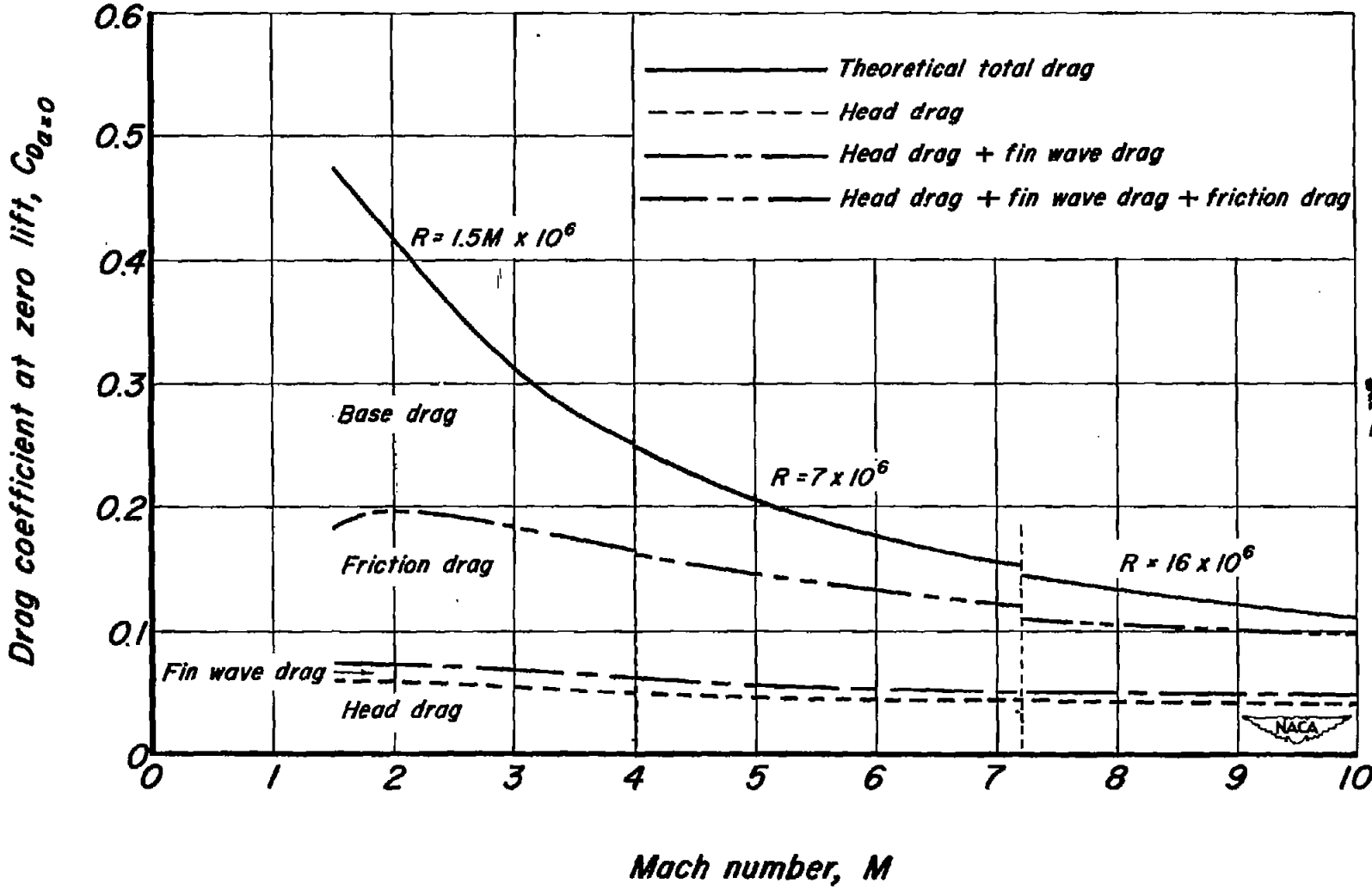

Figure 10. – Summation of theoretical components of zero-lift drag coefficient.

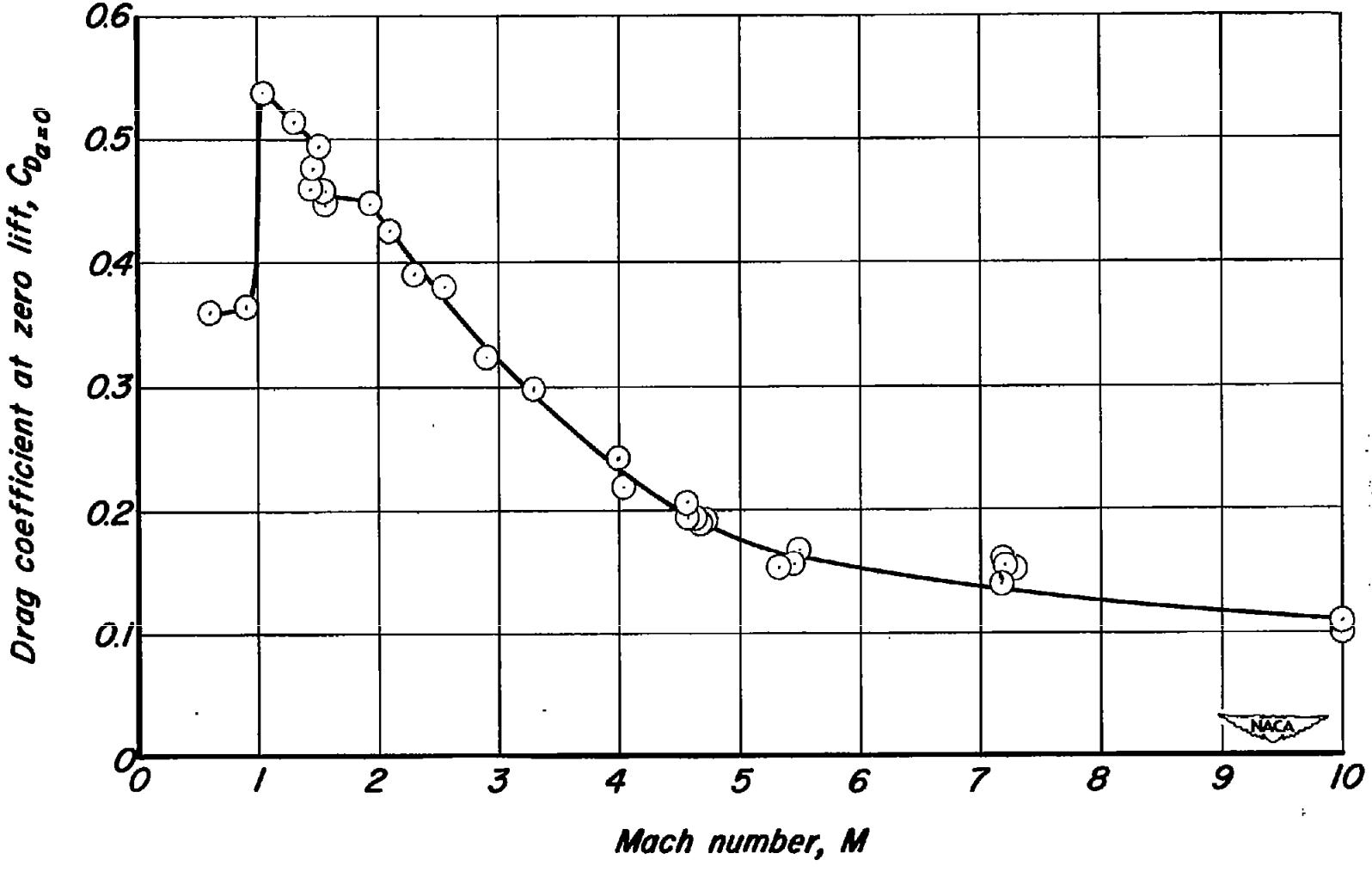

Figure 11.– Experimental variation of total drag with Mach number.

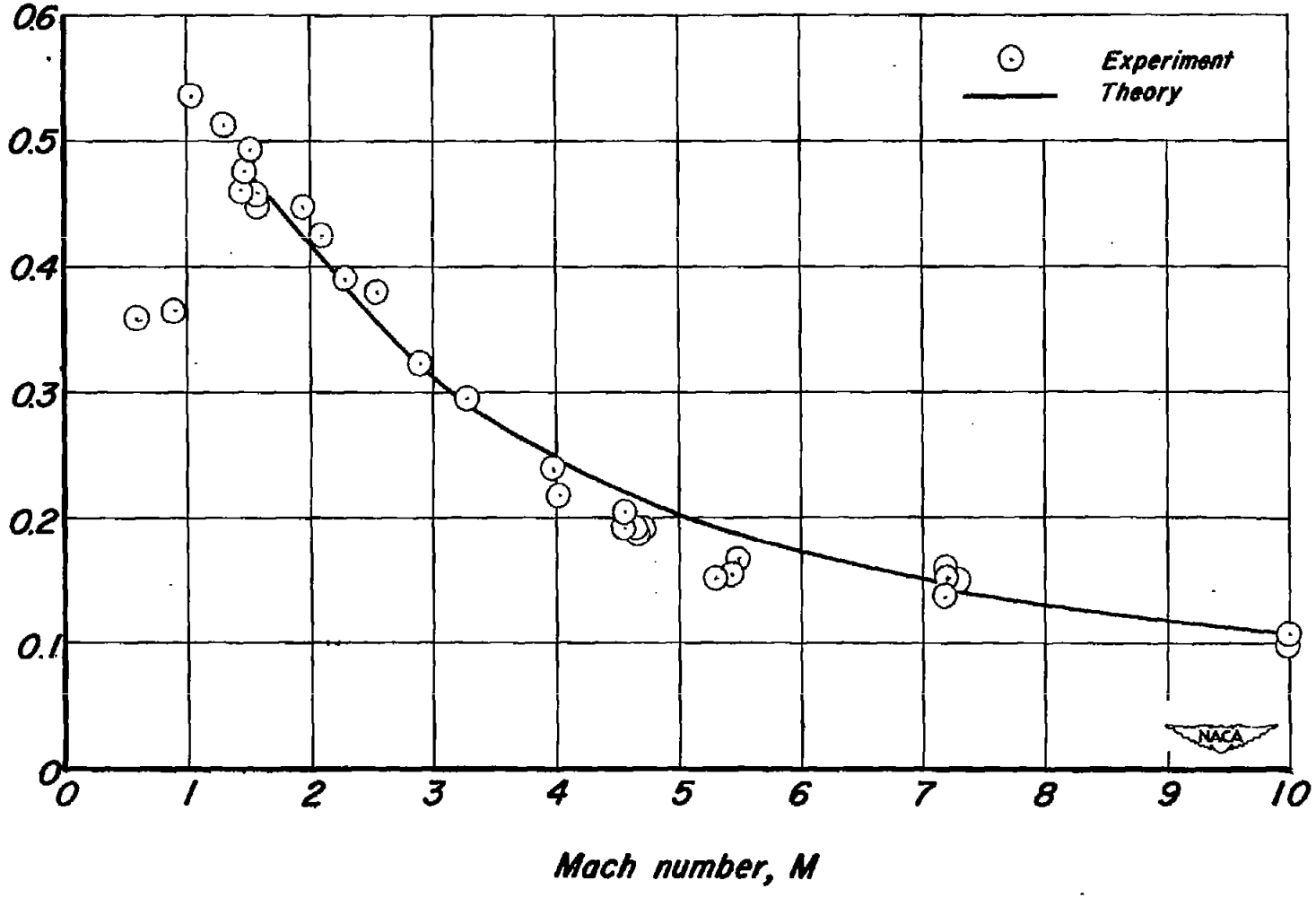

Figure 12. – Comparison of theoretical estimate of total drag with experiment.

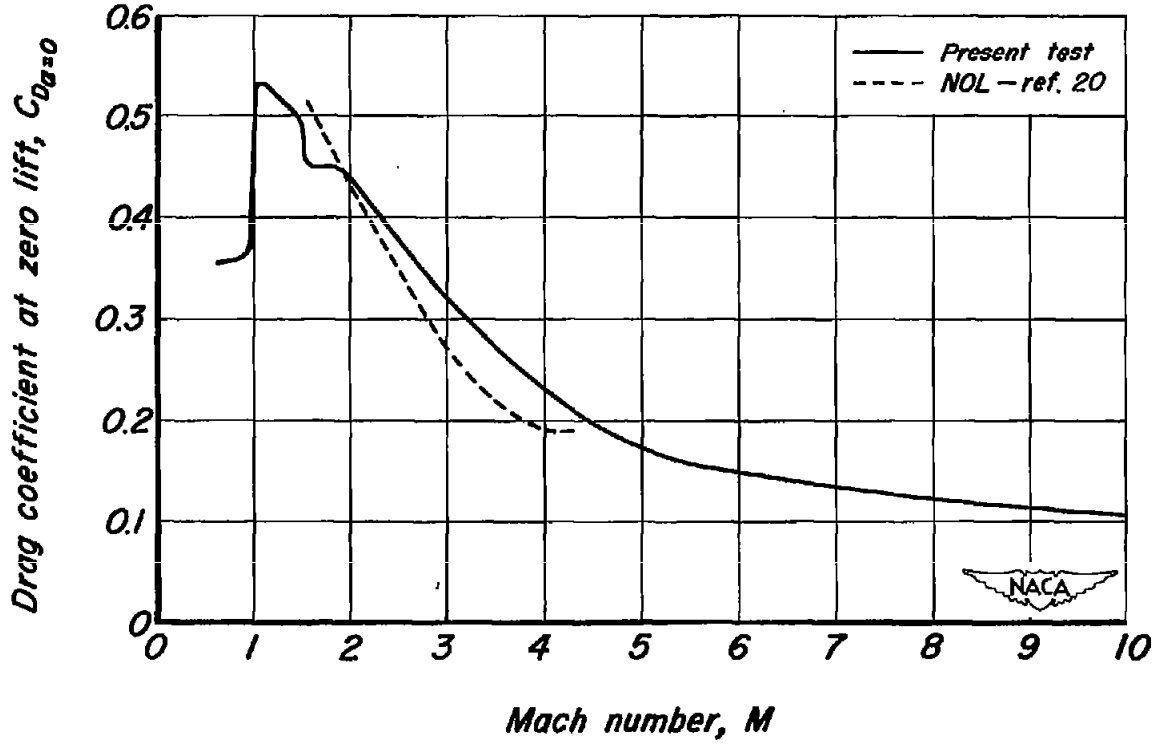

Figure 13. – Comparison of present results with those of reference 20.

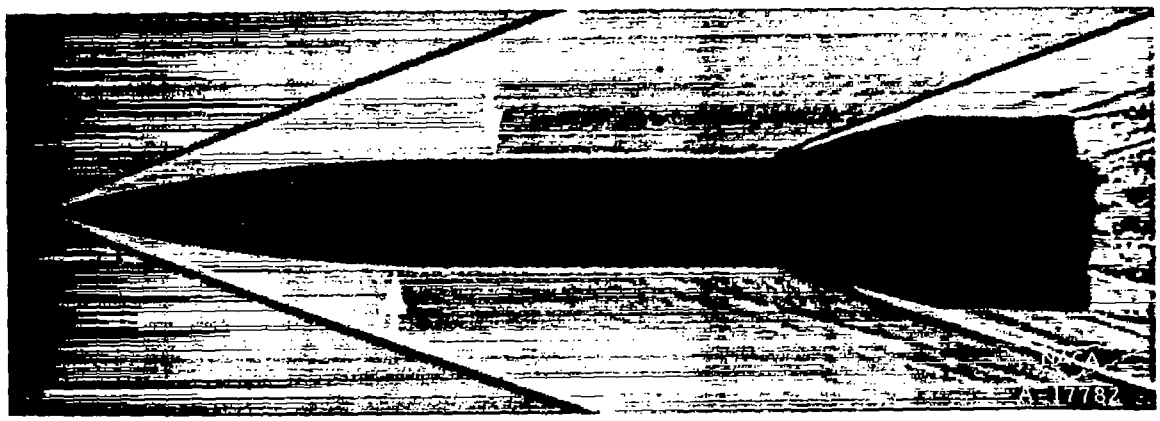

$M = 3.29$; $R = 4.9 \times 10^6$

Figure 14.- Typical shadowgraph from which transition data were obtained. (Arrows indicate beginning of transition.)

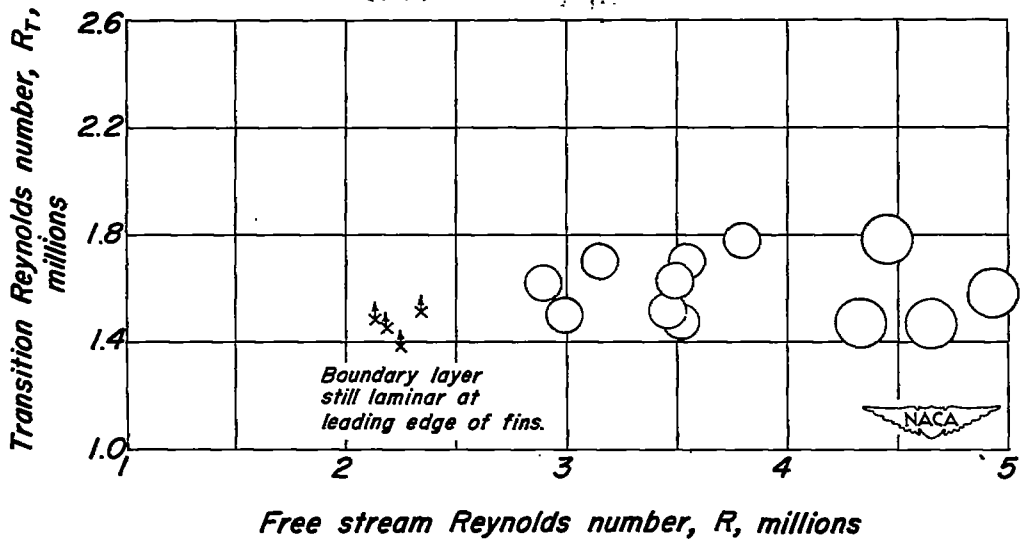

Figure 15.– Variation of transition Reynolds number with free-stream Reynolds number, obtained from air-off data.

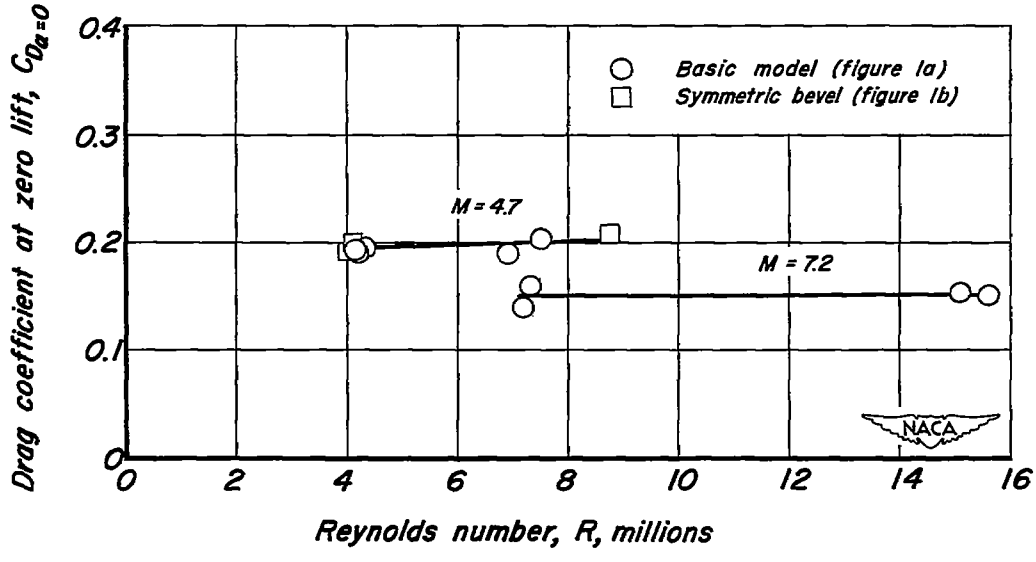

Figure 16.– Dependence of zero-lift total drag coefficient on free-stream Reynolds number.

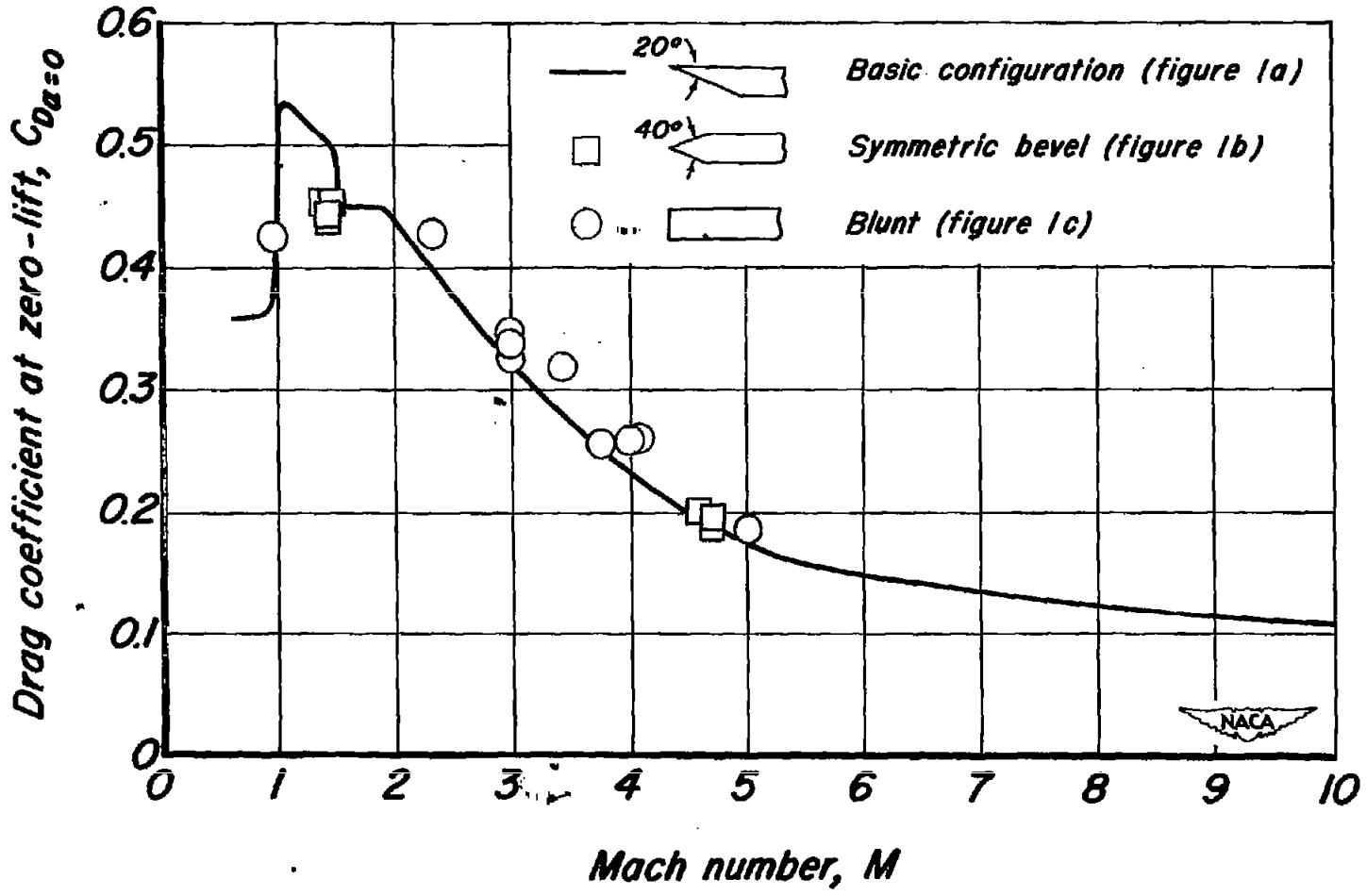

Figure 17.- Effect of fin leading-edge shape on total drag.